Structural damage quantification using long short-term memory (LSTM) auto-encoder and impulse response functions

Chencho [a], Jun Li [a,*], Hong Hao [b,a]

[a] *Centre for Infrastructure Monitoring and Protection, School of Civil and Mechanical Engineering, Curtin University, Kent Street, Bentley, WA 6102, Australia*
[b] *Earthquake Engineering Research and Test Center, Guangzhou University, Guangzhou, China*

ARTICLE INFO

ABSTRACT

This paper presents an approach for structural damage quantification using a long short-term memory (LSTM) auto-encoder and impulse response functions (IRF). Among time domain responses-based methods for structural damage identification, using IRF is advantageous over the original time domain responses, since IRF consists of information of system properties and is loading effect independent. In this study, IRFs are extracted from the acceleration responses measured from different locations of structures under impact force excitations. The obtained IRFs are concatenated. Moving averaging with a suitable window size is performed to reduce random variations in the concatenated responses. Further, principal component analysis is performed for dimensionality reduction. These selected principal components are then fed to the LSTM auto-encoder for structural damage identification. A noise layer is added as an input layer to the LSTM auto-encoder to regularise the model. The proposed model consists of two phases: (1) reconstruction of the selected "principal components" to extract the features; and (2) damage identification of structural elements. Numerical studies are conducted to verify the accuracy of the proposed approach. The results demonstrate that the proposed approach can accurately identify and quantify structural damage for both single- and multiple-element damage cases with noisy measurements, as well as uncertainties in the stiffness parameters. Furthermore, the performance of the proposed approach is evaluated using the limited measurements from a few sensors.

1. Introduction

Damage identification and safety evaluation of civil engineering structures are essential objectives of structural health monitoring (SHM). This is achieved by measuring the responses of structures and the loading conditions for further analysis. The as-obtained data are analysed using data interpretation algorithms. When the data obtained from various sensors are highly complex and heterogeneous, machine learning algorithms can be used for structural condition diagnosis and damage prognosis (Smarsly et al., 2013). Such algorithms generate knowledge about the structures using the structural data from the sensors and numerical data from the simulations (Chencho et al., 2021). Recent evidence shows that machine learning methods are more precise and superior to traditional methods, especially in the case of vague or noise-contaminated data sources (Khan and Yairi, 2018). It can obtain knowledge automatically from the available data.

Vibration-based methods (Rafiei and Adeli, 2018; Wang et al., 2021; Wu and Jahanshahi, 2018) have been extensively developed for SHM to identify and quantify damage based on vibration responses. These methods have been widely used in the health monitoring of machines and their components based on the measured vibration responses such as displacement, strain and acceleration (Heng et al., 2009; Jardine et al., 2006; Kan et al., 2015). Vibration-based methods have also been developed for SHM of civil engineering infrastructure, ultimately overcoming the issues with the traditional structural condition monitoring and safety evaluation of the monitored structures (Avci et al., 2021; Mansouri et al., 2015; Shadan et al., 2016). To examine the ageing and degradation of a bridge, Magalhães et al. (2012) installed force balance accelerometers within the deck box girders to measure both vertical and lateral accelerations. The natural frequency changes over time were monitored with the surrounding temperature to observe possible changes in the bridge's condition status. The natural frequency variation over time with the RMS value of the vertical acceleration and the average day evolution of the modal damping ratios and natural frequency changes during working days were also obtained. A method was proposed to minimize the effects of environmental and operational

---

factors on the natural frequencies, which helped to identify the structural anomalies in the subsequent stage (Magalhães et al., 2012).

Machine learning algorithms have been used together with vibration responses to monitor the health of structures. It has the capacity to explore features in the measurement data and can provide information about the structure's condition. They do not require a high configuration computer system for training and are relatively fast. It has been used for damage identification and localization with time domain measurements, which are mostly the acceleration responses from the structures. It does not require extracting parameters, such as the modal information from the measurements recorded from the sensors. Autoregressive model (AR) and residual error (RE) have been used to extract damage-sensitive features for support vector machine (SVM) by Gui et al. (2017) to detect damage in frame structures using time series measurements. The hyperparameters of SVM were tuned with three different optimization techniques. Numerical results demonstrated the improvement in the performance over the conventional methods in terms of sensitivity, accuracy and effectiveness. Chencho et al. (2021) proposed a random forest-based structural damage identification and quantification method. The time-domain responses were generated using the Finite Element Model (FEM) to train and test the model. Experimental studies were carried out on the frame in the laboratory. The proposed method has shown good damage identification results for both numerical and experimental studies. The study was further extended using an extremely randomized tree and extracted impulse response functions (IRFs) from time-domain response measurements (Chencho et al., 2022).

Artificial neural networks (ANN) were used along with the feature extraction methods for damage identification and localization. A numerical study (Mehrjoo et al., 2008) on a simple Louisville bridge truss was carried out for damage detection of joints using modal characteristics extracted from acceleration responses. Damage was introduced by reducing the truss member's stiffness, and bending modes were used for training the model. The first four modes of truss bridge and five modes of Louisville bridge were used to train the model. The results indicated good damage identification performance. However, the complete training process took 75,000 epochs, which is quite large. An application of Bayesian model class selection to select an optimal ANN model class was proposed for detecting damage in a four-story, 22-bay steel frame with 120 degrees of freedom (Ng, 2014) using modal characteristics of the model under several structural damage states. A combined method (Betti et al., 2015) consisting of ANN and genetic algorithm was developed for structural damage identification of a three-story steel structure. Structural damage was introduced by partial cuts of flanges on a column. Acceleration measurements from undamaged and damaged levels under ambient conditions were recorded to obtain natural frequencies and mode shapes. The minimization of modal characteristics between the experimental and numerical studies using two fitness functions and the damage identification was tested using the genetic algorithm. Studies by Cury and Crémona (2012), Goh et al. (2013), Lee and Lam (2011), and Zhou et al. (2014) have used modal information with machine learning models for damage identification and localization.

A numerical study (Dackermann et al., 2016) using principal component analysis (PCA) with ANN and ensembles of ANN was conducted for the damage identification and localization of a pin-pin supported steel beam. Modal parameters were extracted from the time domain responses, and the modal strain energy-based damage indices were derived. PCA was applied to the damage indicators, and significant principal components were selected as input to the ANN for damage identification and localization. PCA was utilized to reduce the effect of noise, and performance was evaluated against different levels of white noise. A three-stage ANN method for damage assessment of building structures was proposed in the study by Bandara et al. (2013). The first stage determined the damaged floor, and a specific damaged element was identified in the second stage. The damage severity was identified in the third stage. The study was carried out on a numerical model of a 10-storey frame structure with the frequency response function obtained from the acceleration measurements. The result indicated that the PCA-based damage index was suitable for structural damage detection. PCA was used with noise filtering for feature extraction. Some researchers (Abdeljaber and Avci, 2016) proposed a nonparametric structural damage detection method using self-organizing maps to extract damage indices from ambient acceleration measurements. The study was conducted to identify and locate damage due to stiffness reduction and change in boundary conditions of a numerical model of a hot-rolled steel grid structure.

Deep learning models have been extensively used for the damage identification and quantification of civil engineering structures. It is a subset of machine learning methods, and it can learn from the data in an unsupervised manner and extract the optimal input representation from the raw data without the intervention of the user. Thus, deep learning models can learn not only how to correlate features to the desired output, but also how to extract features (Avci et al., 2021) unlike in parametric and nonparametric methods discussed above. An ensemble classification method for structural damage assessment was proposed using FRF generated from a numerical model (Fallahian et al., 2017). A deep neural network and a couple of sparse codes are two classifiers used for the damage classification, and the decision is made based on the majority voting. The input to the classifiers is the features extracted by using PCA. The numerical study was carried out on a truss bridge with 25 elements and validated with data obtained from the I-40 bridge. Good damage classification results were provided, considering temperature variations. Bai et al. (2023) proposed an image and frequency information-based deep learning method for structural health monitoring and post-earthquake reconnaissance. A cost-effective deep learning-based method (Wang and Su, 2023) for detecting and classifying the condition of the bearings of a bridge was proposed. The study developed two models: one for detecting the bearing (BearDet) using a transformer network for feature extraction and a deep learning model for accurately classifying (BearCla) the condition of the bearing. A method for detecting pavement defects based on convolutional neural networks using grey and depth images was proposed by Li et al. (2024). Classic U-shape and double-headed structures were developed to accommodate the image data characteristics. The detection accuracy of the proposed model was enhanced by integrating attention models. The use of a two-dimensional convolutional neural network (CNN) for four damage states prediction using the acceleration responses recorded during the shake table testing of a reinforced concrete highway bridge model was proposed by Khodabandehlou et al. (2019). A deep residual network for structural damage identification using the modal information was proposed by Wang et al. (2020). Both the numerical and experimental studies provided good structural damage identification results. However, the use of modal information requires more sensor measurements. Furthermore, the computational demand of two-dimensional CNN and deep residual networks is more expensive.

Auto-encoders perform hierarchical non-linear mapping to learn features that represent datasets (Vincent et al., 2010), and have been also used for dimensionality reduction. In studies by Fallahian et al. (2017), Fallahian et al. (2018), Pathirage et al. (2019), and Wang et al. (2018), autoencoders have been used for damage identification and quantification. Recent studies on structural damage identification and localization with auto-encoders used the natural frequencies and mode shapes as the input, and the stiffness reductions in structural elements as the output. A number of sensor measurements were required at several locations of the structure to obtain accurate modal information such as mode shapes (Chencho et al., 2021; Wang et al., 2021). This can be expensive because of the costs incurred on long cables and many sensors and data acquisition systems. Using time domain responses can overcome the issue with the use of a large number of measurements to obtain modal information for damage identification and localization. Abdeljaber et al. (2017) proposed a real-time damage detection and

localization method using adaptive one-dimensional (1D) CNN and raw signal measurements with accelerometers. Wang et al. (2021) used only a few sensors and time-domain responses and achieved excellent damage identification and quantification results by using densely connected neural networks. Chencho et al. (2021) conducted a similar study using principal component analysis (PCA) and an ensemble-based machine learning algorithm, namely, the random forest. Good damage identification and quantification results were close to those from the deep learning models at a relatively low computational cost. PCA has been used to extract information from high dimensional data. Such data can be represented using a few principal components that retain most information (Sarbu and Pop, 2005), and the process is faster than auto-encoder when used for the dimensionality reduction.

Further, IRF is one of the dynamic properties of structures and can be extracted from time domain responses. IRF is an inherent system property, therefore it is more advantageous than using the measured time domain response. In studies of Li and Law (2008) and Robertson et al. (1998), the estimation of IRFs using discrete wavelet transform has been discussed. It can be analytically derived from general equation of motion (Law and Li, 2007; Li et al., 2015). Li et al. (2015) proposed a structural damage identification method that used a sensitivity-based method and the impulse response functions (IRFs) extracted from the acceleration responses. Lin et al. (2019) proposed a method to estimate IRF from structural responses recorded from multiple unknown excitations and utilized IRF for structural damage identification and quantification. An equivalent single excitation problem was obtained for multiple general excitations, and IRFs were estimated using wavelet-based and regularization-based method. The performance was measured with and without considering noise containment in the measured data for a numerical model of a simply supported plane truss. Smith and Hernandez (2019) explored the use of impulse response sensitivity and least absolute shrinkage and selection operator (LASSO) regularization for sparse damage detection in terms of stiffness reductions in a numerical model of a non-uniform shear beam with noisy measurements, limited model parameters and limited sensor locations. The results demonstrated that sparse damage can be detected by using the changes in identified impulse responses.

This paper proposes a structural damage identification approach using long short-term memory (LSTM) based auto-encoders and IRFs. The proposed approach uses IRFs extracted from the acceleration responses under impact excitations measured at the selected nodes of the structure. The extracted IRFs are concatenated, and PCA is performed for dimensionality reduction, which helps to reduce the overall computational cost of using the LSTM auto-encoder for structural damage identification. Numerical studies are conducted on a simply

supported beam, and datasets are generated using finite element model analysis for verifying the performance of the proposed approach. In this study, the proposed LSTM auto-encoder is explored for structural damage identification by considering input as one sequence and output as another sequence. This study: 1) implements a LSTM auto-encoder for structural damage identification, and the model does not need to be trained and tested for different damage scenarios as in other structural elemental damage identification; and 2) explores IRFs extracted from time domain acceleration responses using only a few sensors. The identification results demonstrate the performance of the proposed approach by using only a few sensor measurements.

2. LSTM auto-encoder

LSTM has been widely used in sequence prediction problems, such as sequence classification and sequence-to-sequence prediction, which may differ based on the input and output sequences. LSTM is a type of recurrent neural network (RNN). It has recurrent connections that use the state of neuron activation from the previous time step to determine the output (Brownlee, 2017). RNNs are designed for sequence prediction, for example, multi-layer perceptron adding loops. RNNs face the challenge of getting trained effectively owing to vanishing gradient problems. LSTM is designed to overcome this challenge. Moreover, LSTM can learn long-term dependencies better than an RNN (LeCun et al., 2015). LSTM uses gates that process the information contained in the incoming data sequences. The gates include a forget gate, an input gate and an output gate, each of which can be considered a neural network (Xu and Yoneda, 2021; Zhang et al., 2020). The output from an LSTM cell depends on the long-term memory (referred to as the cell state), output from the previous time step, and data of the input sequence of the current time step. Fig. 1 shows a typical example of an LSTM cell.

The forget gate determines which information of the cell state is useful based on the previous hidden state and the current input data. The previous hidden state and the current input data are fed to the forget gate, generating a vector between 0 and 1 using sigmoid activation. A value of 0 indicates that the input component is irrelevant, whereas 1 indicates the input component is relevant. In the following equations, W and W_h are the input and hidden state weights for the forget gate f, input gate i, and output gate o.

$$f_t = \sigma\left(x_t \times W_f + h_{t-1} \times W_{hf}\right) \tag{1}$$

where x_t, h_{t-1} and f_t denote the data at time instant t, the previous hidden state, and the forget gate at t, respectively. σ is the sigmoid activation
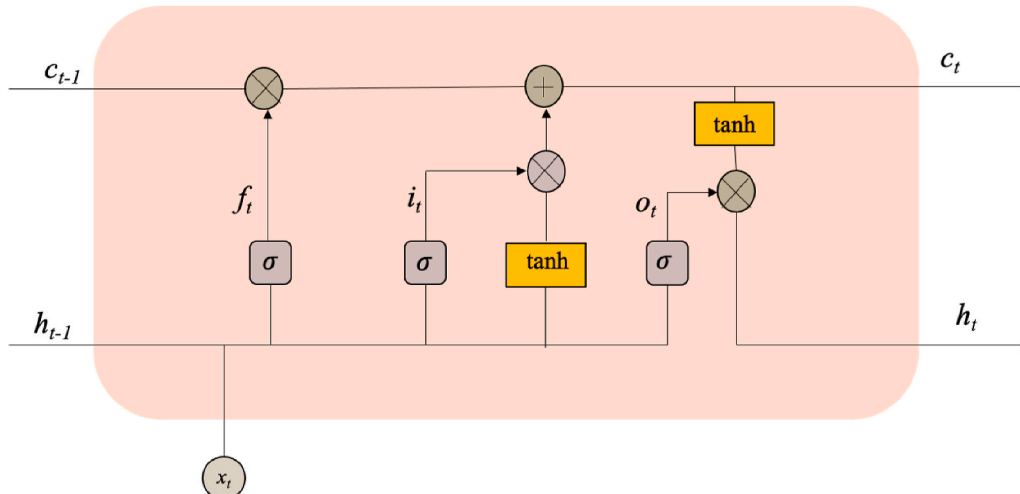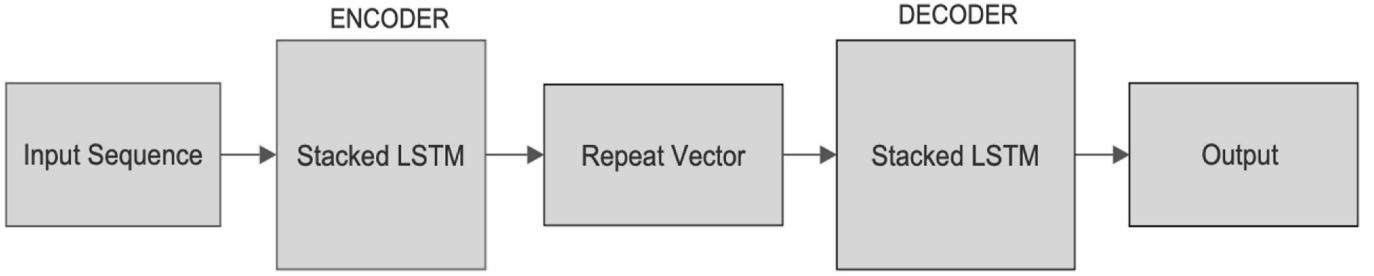

Fig. 1. An example LSTM cell.

Fig. 2. LSTM auto-encoder.

function. The input and hidden state are multiplied by the weights. The weight matrix remains the same and it does not change from one time step to another.

The amount of information sent is based on this value. More information is sent when the value is closer to 1. The output from this part of the forget gate is multiplied pointwise by the previous cell state. The output of pointwise multiplication is given by Eq. (2) or Eq. (3) when f_t is 0 or 1, respectively. When it is 1, all previous cell states are sent.

$$C_{t-1}*f_t = 0 \, for \, f_t = 0 \tag{2}$$

$$C_{t-1}*f_t = C_{t-1} \, for \, f_t = 1 \tag{3}$$

where C_{t-1} denotes the previous cell state.

The next stage is the input gate. The input gate uses the current input and the previous hidden states to quantify the amount of new information to be retained along with the previous cell state. The equation for the input gate can be expressed as

$$i_t = \sigma(x_t \times W_i + h_{t-1} \times W_{hi}) \tag{4}$$

where i_t is the input gate at time instant *t*.

Using a sigmoid function, the input gate outputs a vector ranging from 0 to 1. The new information is a function of the previous hidden state and current input data. It uses the "*tanh*" activation function to output the new information ranging from −1 to 1. The new information is determined as:

$$I_N = tanh(x_t \times W_c + h_{t-1} \times W_{hc}) \tag{5}$$

The new information generated using the input gate can help to reduce the previous-state information in the cell state, if necessary. A negative value using the activation function "*tanh*" helps to achieve this. However, the necessity of retaining all the new input data is unknown. The output from the input gate is multiplied pointwise by the new input vector to determine the amount of new input data that can be retained. This output is added to the cell state. The current cell state is given as:

$$C_t = C_{t-1}*f_t + I_N*i_t \tag{6}$$

The output gate is the last gate, which determines the new hidden state. It uses the current input data and previous hidden state, similar to the forget and input gates. The equation for the output gate can be expressed as:

$$o_t = \sigma(x_t \times W_0 + h_{t-1} \times W_{ho}) \tag{7}$$

The new hidden state is the output of the pointwise multiplication of the value of the output gate and new cell state. The "*tanh*" activation function is applied to the current cell state, resulting in a new output ranging from −1 to 1. The new hidden state can be expressed as:

$$h_t = \sigma(x_t \times W_o + h_{t-1} \times W_{h0})*tanh\,(C_t) \tag{8}$$

LSTM auto-encoder is an LSTM-based architecture (also referred to as encoder–decoder LSTM), as shown in Fig. 2. The encoder reads the input sequence and encodes it into a vector (Hochreiter and Schmidhuber, 1997). The decoder decodes this vector and outputs the predicted sequence.

3. Proposed network configuration

The proposed LSTM auto-encoder consists of two phases. Fig. 3 shows the proposed network, which is implemented using Keras Functional API (Chollet, 2019) for deep learning. The first phase involves reconstructing the input sequence to extract the best feature representing the input sequence, and the second phase involves relationship learning for structural damage identification. A network may learn effectively from a training dataset to train the input samples and the corresponding outputs, but it may perform poorly on new datasets, such as testing and validation datasets. This results in a generalisation error, which can often be improved by adding random noise, resulting in less effective network learning of the training dataset (Brownlee, 2019). The Keras API enables the addition of white noise to the network via a Gaussian layer, as shown in Fig. 3.

Adding a Gaussian layer adds noise with a mean value of zero. The standard deviation of noise can be tuned to obtain the best results for the network. A standard deviation of 0.3 is used for the proposed network, and the Gaussian layer is added as an input layer to the encoder. The encoder outputs internal representations of the input sequences. The input to the network for both networks requires 3-dimensional input of [samples, timestep, features]. Here, "samples" denotes the observation, "timestep" is the sequence length and "features" is the number of features in the input. Both the encoder and decoder are stacked LSTM networks. A stacked LSTM network has multiple hidden layers, each with multiple memory cells. The output from the encoder is of 2-dimensional output and decoder, which is also a stacked LSTM network requiring 3-dimensional input. The repeat Vector layer is used here to create 2-dimensional output from the encoder to 3-dimensional data for the decoder. The decoder maps the learned internal representation of the input sequence to the output sequence. A dense layer is used as the output for the network.

In the first phase, the encoder and decoder are tuned to obtain the maximum R-squared value for reconstructing the input sequence. The input sequence is the PCA-compressed IRFs. IRFs are extracted from acceleration measurements from the structure. IRF extraction is described in Section 4. The decoder uses the learned internal representations of the input signal by the encoder as the input to reconstruct the input sequence. The encoder and decoder are tuned to obtain a good reconstruction of the input sequence from the decoder. The damage identification network is developed using the same encoder when the maximum R-squared is achieved for reconstructing the input sequence.
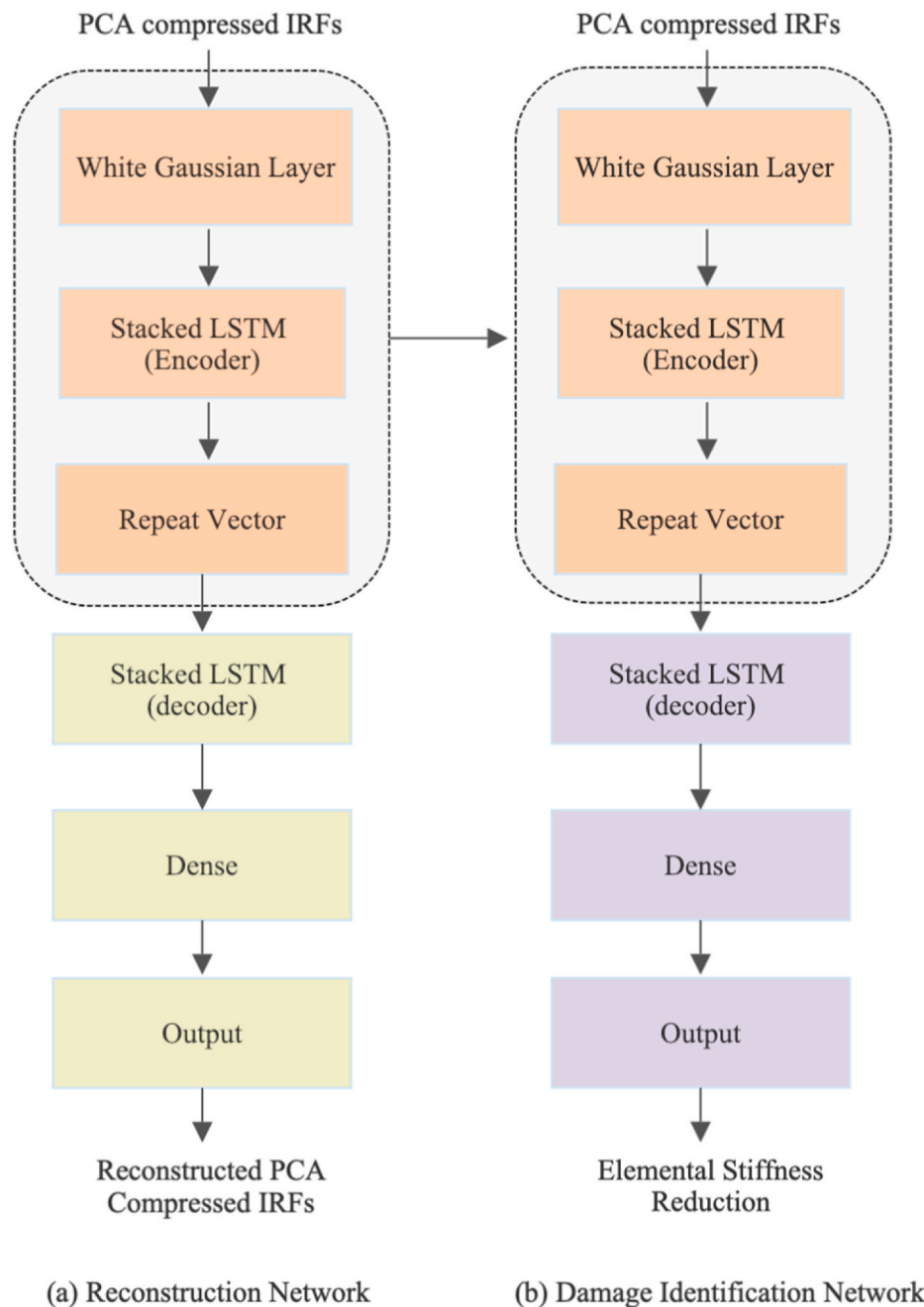
Fig. 3. The proposed network.

The output is to predict structural elemental stiffness reduction. Using the same encoder and a decoder of the damage identification network is tuned to obtain good damage identification results. Therefore, in the damage identification phase, the learned internal representation of the input sequence is mapped to stiffness reduction. Fig. 3(b) shows the damage identification network.

4. Data generation and pre-processing

Numerical studies are conducted on a supported beam to validate the accuracy and performance of the proposed approach. Young's modulus of 3.3×10^4 MPa is considered initially for finite element modelling. The beam is 20 m long, 0.6 m wide, and 1 m high. The mass density is 2500 kg/m^3. There are 11 nodes, and only the vertical acceleration responses from the selected nodes are used. Impact forces are applied at node 3 to generate the study's required acceleration responses. Fig. 4 shows the beam structure and the selected sensor locations.

The datasets used in this study are generated by finite element analysis. The acceleration responses are measured at the sampling rate of 100 Hz when an impact force with a duration of 0.1s is applied at node 3. The acceleration response with a duration of 1s from the randomly selected sensor locations is used for the study. The dataset is generated for both damaged and undamaged cases. The damage is defined in terms of the percentage stiffness reduction in structural elements and introduced by reducing the stiffness parameter, namely, Young's modulus. For the damaged case, data are generated considering single-element, two-element, and three-element damage cases. A maximum stiffness reduction of 20% in steps of 0.5% for the single-element damage case and 15% in steps of 1.5% for all two-element damage cases are considered. For every three-element damage case, the minimum and
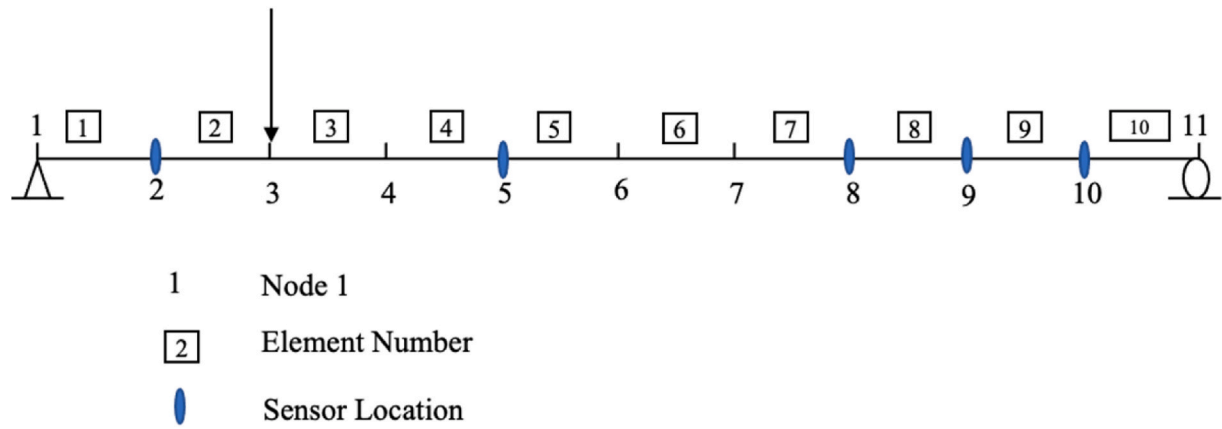
Fig. 4. Simply supported beam and sensor locations.

maximum stiffness reductions of 1.5% and 15% are considered in steps of 4.5%. Every sample has "*n'*"outputs, where "*n*" is the number of elements. The output indicates the percentage of stiffness reduction for each element. Initially, the responses are measured from the five selected nodes under random impact forces generated by a Gaussian distribution with a mean of 8 kN and a standard deviation of 0.05 kN.

The IRF is extracted using Eq. (9) based on the existing studies (Li et al., 2015) as follows

$$H = X \times \left(F^T \times F\right)^{-1} \times F^T \qquad (9)$$

where *H* denotes the IRF vector, *F* denotes the excitation force matrix, and *X* denotes the acceleration response vector. It should be noted that the pseudo-inverse is used to extract the impulse response function. Normally, the condition number for the excitation force matrix is not an extremely large value since the columns are basically independent. However, when the matrix is badly ill-conditioned, the truncated Singular Value Decomposition (TSVD) can be employed to eliminate those very small singular values and the corresponding vectors for a better and more stable solution for the pseudo-inverse. The error in the IRF is reduced by averaging the results obtained using 50 ensembles. The IRFs extracted from the five sensor locations are concatenated, resulting in a sequence length of 500 sample points. Moving averaging is performed with a suitable window size to remove random variations. However, the sequence length (500) is considerably high for LSTM, which can increase the computational cost of the LSTM network. Therefore, PCA is performed on the concatenated input sequence to reduce the sample length to minimise the overall computational cost. Nineteen principal components are selected, with the minimum total variance of 98.71% of the data preserved when selecting the number of principal components. These 19 principal components are used as the input sequence to the LSTM auto-encoder network. Therefore, the input to the LSTM auto-encoder comprises 19 time steps, which are the 19 principal components. The entire dataset is reshaped into [samples, timesteps, features].

This study considers noisy measurements and uncertainties in system modelling. Damage in the structural elements is defined as stiffness reduction, that is, a reduction in the stiffness parameter, i.e., Young's modulus. All ten elements would not have the same Young's modulus values because of unavoidable uncertainties in the material properties and manufacturing quality. Accordingly, four scenarios are considered for investigating the performance of the proposed approach.

Scenario 1: Acceleration responses measured from selected sensor locations are used without considering noise or uncertainty. The IRFs are extracted from these measured responses.

Scenario 2: White noise is added to acceleration responses recorded in Scenario 1. The IRFs are extracted from the acceleration responses along with noisy measurements. Two different levels of white noise, 5% and 10%, are considered to determine the effect of the noise level on the performance.

Scenario 3: Acceleration responses measured with uncertainty. Uncertainty ranging from ±1%–3% is included randomly in the stiffness parameters in the FEM. The IRFs are extracted from the acceleration responses. No noise measurements are considered herein.

Scenario 4: Acceleration responses are measured considering the uncertainty and noise measurements. Acceleration responses are measured, including uncertainties ranging from ±1%–3%. 5% and 10% noise are added to the measured acceleration responses, and the IRFs are extracted.

Only the IRFs extracted from Scenarios 1 and 3 are used for training and testing the framework. For Scenario 1, 11,300 single- and multiple-element damage cases are simulated. Three samples are generated for each damage case under a different impact force. For the same damage cases, uncertainty (ranging ±1%–3%) is included in the stiffness parameter, and the acceleration responses are measured, from which the IRFs are extracted and considered as Scenario 3. Scenarios 1 and 3 had the same damage cases (11,300). Both scenarios are combined to yield 22,600 damage cases, and with three samples for each damage case, 67,800 samples are generated. Four undamaged samples are added to the dataset, forming the final dataset with shape [67804, 19, 1] for the study.

Scenarios 1 and 3 are combined to train and test the proposed framework. The network is trained using 85% of the entire dataset. The remaining 15% is used as one set for testing the proposed model. Fifteen per cent of the training dataset was used to validate the proposed method. Three sets of test data are used to test the performance of the proposed method.

   i. Random 15% of the dataset to test Scenarios 1 and 3
  ii. Scenario 2 dataset
 iii. Scenario 4 dataset

5. Results and discussions

During the reconstruction phase, the first 19 principal components are used as the input sequence to the LSTM auto-encoder, and the same sequence is used as the output for the reconstruction. The first and second principal components are considered as the values for the first- and second-time steps, respectively. The numbers of LSTM cells and layers in the encoder and decoder are tuned to obtain the maximum R-squared for the validation dataset. The reconstruction network is compiled using the Adam optimiser by considering mean square error (MSE) as the loss function. An R-squared of 0.996 is achieved with the reconstruction network configuration. Table 1 presents the results of the reconstruction of two random samples, and the reconstructed sequence is almost the same as the input sequence.

Table 1

Input sequence and reconstructed sequences.

Time steps	Sample 1		Sample 2	
	Input seq.	Reconstructed seq.	Input seq.	Reconstructed seq.
1	−9.05	−9.07	−11.31	−11.24
2	1.70	1.69	−10.72	−10.72
3	−0.68	−0.68	6.77	6.89
4	−1.49	−1.52	5.00	5.07
5	0.89	0.84	0.99	0.89
6	0.10	0.11	1.16	1.26
7	−1.24	−1.24	−1.83	−1.88
8	−1.97	−1.98	2.27	2.25
9	0.87	0.83	−1.62	−1.65
10	−0.28	−0.29	−1.26	−1.31
11	0.05	0.02	−1.19	−1.19
12	0.32	0.35	−0.59	−0.57
13	0.06	0.10	0.37	0.29
14	−0.09	−0.10	−0.17	−0.24
15	0.21	0.19	0.38	0.41
16	−0.72	−0.69	0.02	0.03
17	0.11	0.10	−0.69	−0.66
18	−0.22	−0.19	0.39	0.33
19	−0.12	−0.12	−0.07	−0.03
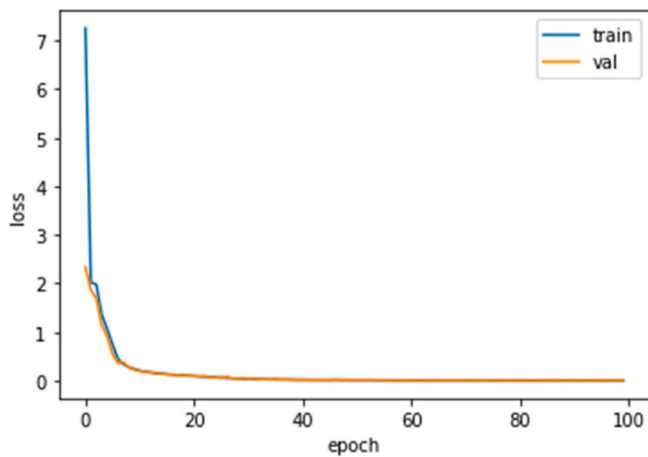
Fig. 5. Loss curve for reconstruction network.

Table 2

Performance measurements of the proposed method using five sensor measurements.

Performance metrics	Scenario 1	Scenario 2	
		5% noise	10% noise
MSE	3.21×10^{-6}	6.15×10^{-6}	2.5×10^{-5}
R-squared	0.998	0.996	0.985

The learning plot for the reconstruction network over 100 epochs is shown in Fig. 5. The plot provides information on the network performance of the training and validation datasets and can be used to determine whether the network underfits, overfits, or learns well. The training curve (obtained from the training datasets) provides

Table 3

Performance measurements using five sensor measurements for Scenarios 3 and 4.

Performance metrics	Scenario 3	Scenario 4	
		5% noise	10% noise
MSE	4.16×10^{-5}	4.9×10^{-5}	7.08×10^{-5}
R-squared	0.974	0.971	0.953
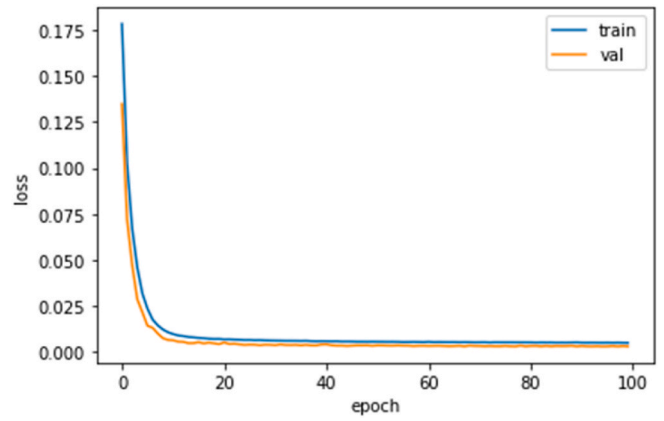
Fig. 6. Loss curves of the damage identification network.

information on the learning performance of the proposed network. In contrast, the validation curve (calculated for 15% of the total datasets) provides information on the generalisation performance of the trained network. The plot shows that training and validation losses decrease up to their respective stability points; a small gap exists between the training and validation loss curves. These results indicate a good fit.

After achieving an R-squared value of 0.996, the decoder of the reconstruction network is replaced with another stacked LSTM network. The decoder is tuned further to map the features extracted by the encoder to stiffness reduction. However, the same decoder, which comprised a layer less than that in the reconstruction network, yields good results. The performance of the LSTM auto-encoder in damage identification is measured using the MSE and R-square for the scenarios. For Scenario 2, 5% and 10% noises are considered to investigate the effect of the measurement noise. Table 2 lists the MSE and R-squared for Scenarios 1 and 2. Table 3 shows the results for Scenarios 3 and 4. The proposed method exhibits good damage-identification performance. The performance is slightly affected when noise is present in the acceleration response. The performance further degrades with the increasing noise level. The learning curve for damage identification is shown in Fig. 6, which indicates a good fit.

The R-squared decreases by 0.2% and 1.3% at 5% and 10% noise levels, respectively. When uncertainty is considered without noise measurement in the acceleration responses, as in Scenario 3, the R-squared decreases by 2.4%. With both noisy measurement and uncertainty effect, the performance degrades further, depending on the noise level. Decreases of 2.7% and 4.6% in R-squared values are observed at 5% and 10% noise levels, respectively. Some negative stiffness reductions are observed in the non-damaged elements but are nearly zero. This behaviour has been observed in other deep-learning models (Pathirage et al., 2018; Wang et al., 2018, 2020) used for structural element damage identification with modal information and time-series data.

The damage identification results for the single- and multiple-element cases for all considered scenarios are presented below. Damages with smaller and greater than 10% stiffness reductions are defined herein as minor and major damages, respectively. Fig. 7 shows the damage identification results for the single-element damage case with a 7% decrease in the stiffness reduction in the 4th element. The predicted damage is 6.75% when no noise measurement is considered. Using the data smeared with 5% and 10% noise, the predicted damage identification results are 6.03% and 5.87%, respectively. In Scenario 3, the predicted result is 8.8%. The performance degrades when both the uncertainty and noisy measurements are considered. With uncertainty and 5% and 10% noise levels in measured data, the predicted results are 9.09% and 9.24%, respectively. Some false positive damage identification results are observed in the undamaged elements, but the values are less than 0.5%.

Fig. 7. Damage identification results of a single-element minor damage case in four scenarios.
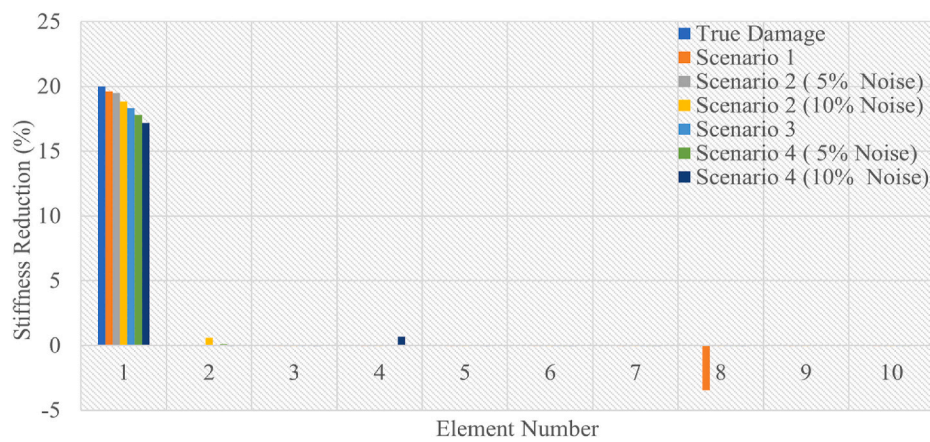
Fig. 8. Damage identification results of a single element with large damage.
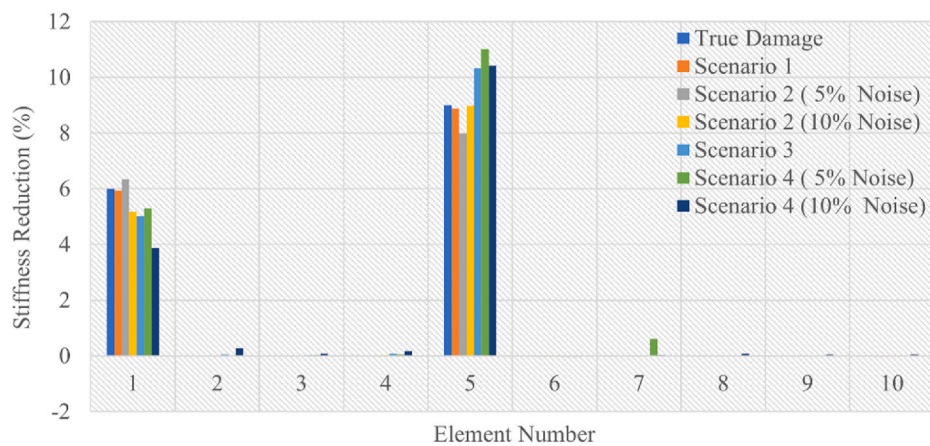
Fig. 9. Damage identification results of a two-element minor damage case.

Fig. 8 shows the single-element damage identification results with a 20% stiffness reduction in the first element under different scenarios. In all the scenarios, the introduced damage can be reliably identified. The performance degrades with an increase in the noise level and degrades further when uncertainty is considered.

Two and three element damages are considered for the multiple-element damage cases. In Fig. 9, stiffness reductions are observed in elements No. 1 and 5. True damages of 6% and 9% stiffness reductions are considered for elements 1 and 5, respectively. Fig. 9 shows the

damage identification results in another two-element damage case. The stiffness reductions are 13.5% for element 1 and 12% for element 6. These figures show that the proposed approach obtains good damage identification results. The identification results are good even when the measurement noise and uncertainty in the stiffness parameter are considered. Very few and small false positive stiffness reductions are observed in Fig. 10.

For a three-element minor damage case, stiffness reductions of 6%, 10.5%, and 6% are introduced in elements 2, 4, and 7, respectively. For a
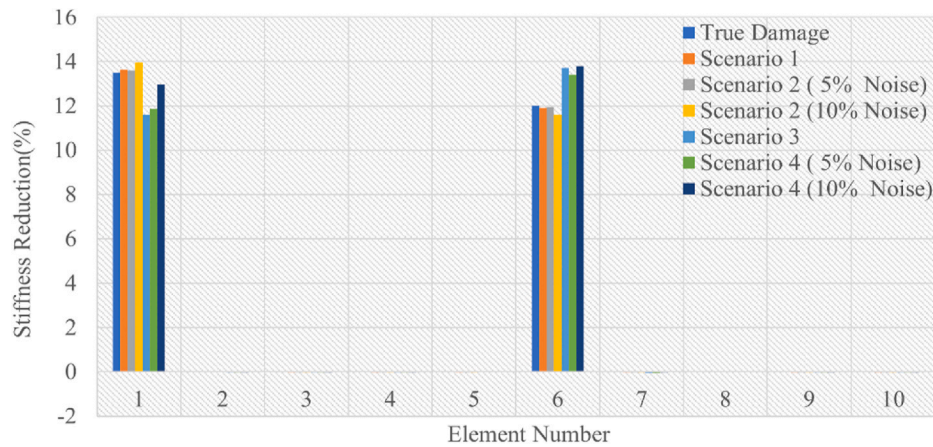
Fig. 10. Damage identification results of a two-element damage case with more than 10% stiffness reductions.
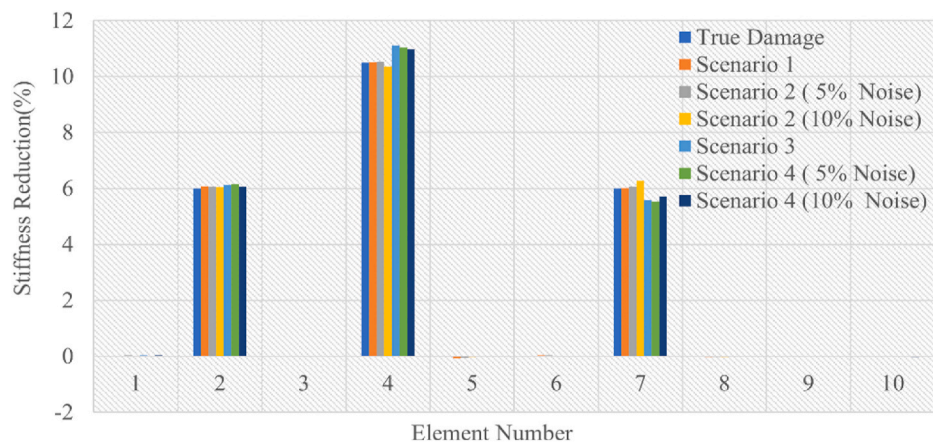
Fig. 11. Damage identification results of a three-element minor damage case.
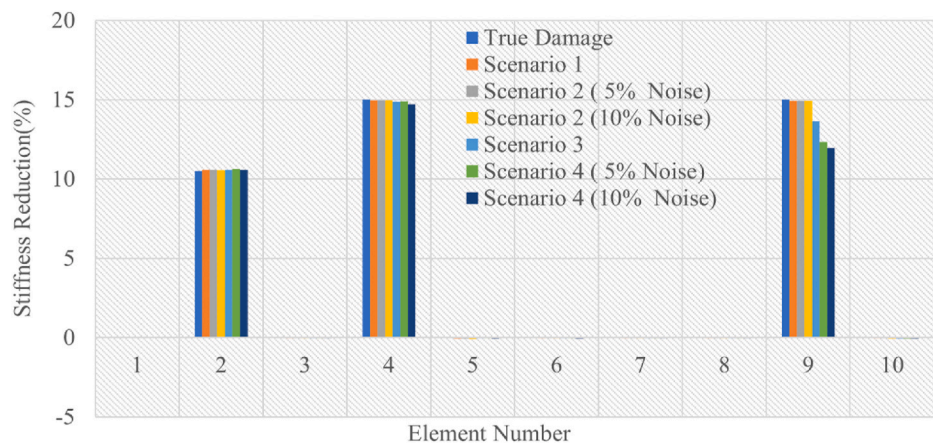
Fig. 12. Damage identification results of a three-element major damage case.

major damage case, the stiffness reductions are 10.5%, 15%, and 15% for elements No. 2, 4, and 9, respectively. The identification results for minor and major damage cases are consistent with those in the single- and two-element damage cases. Fig. 11 and 12 show the identification results for the minor and major three-element damage cases. The prediction results for both single- and multiple-element damage cases are quite close to those of the true damages, even when the measurement noise and uncertainties in the stiffness parameter of the elements are considered.

Next, the number of sensors is reduced from five to three. The vertical acceleration responses are measured from three sensors at nodes 2, 8 and 9, and these responses are processed similarly to the above cases of using five sensors. The same damage cases are used in the training, validation and testing datasets of the above case with five sensors. The 19 principal components selected from the concatenated IRFs are used as inputs to the network with the same architecture, and the performance is measured. The variance retained for the case using five sensors is 98.71% with 19 principal components. When the sensor number is
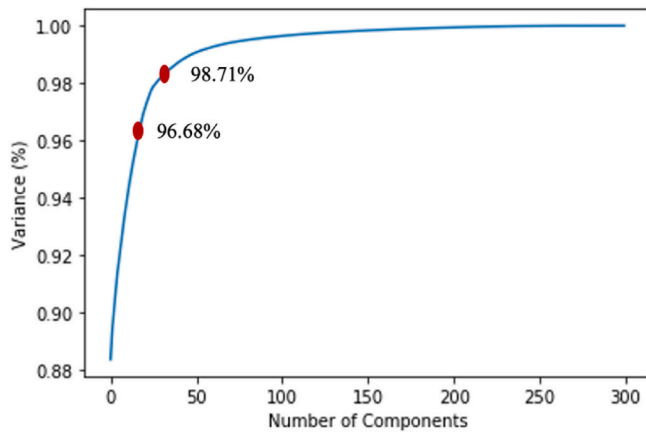
Fig. 13. Variance plot.

Table 4
Performance measurements using three sensor measurements for Scenarios 1 and 2.

Performance metrics	Scenario 1	Scenario 2	
		5% noise	10% noise
MSE	5.7×10^{-6}	8.5×10^{-6}	2.7×10^{-5}
R-squared	0.996	0.994	0.984

Table 5
Performance measurements using three sensor measurements for Scenarios 3 and 4.

Performance metrics	Scenario 3	Scenario 4	
		5% noise	10% noise
MSE	5.3×10^{-5}	6.21×10^{-5}	8.69×10^{-5}
R-squared	0.967	0.961	0.945

reduced to three, with 19 principal components, 96.68% variance is preserved. The proposed approach is trained and tested using 19 principal components. It is observed that the proposed approach can still give good damage identification as those using five sensor datasets. However, as presented in Fig. 13 and 40 principal components must be considered if the number of principal components is selected to retain 98.71% using three sensors. This will increase the training time of the proposed model since the sequence length is more than twice the length using five sensors.

Tables 4 and 5 present the performance measurements of using the proposed approach with three sensor measurements only. R-squared and MSE values are calculated for all scenarios considered in the five-sensor measurement case. Both the MSE and R-squared values indicate good damage identification results. The results are close to those obtained using the five-sensor measurements.

Figs. 14–16 show the comparative damage identification results for Scenario 1 using five- and three-sensor measurements. The introduced stiffness reduction in the element 5 is 9.5%. The predicted stiffness reductions are 9.18% and 9.07% when using data from five and three sensors, respectively. For a randomly selected two-element damage case, the actual stiffness reductions are 13.5% for element 2 and 6% for element 8. The predicted stiffness reductions are 13.3% for element 2 and 5.91% for element 8 (five sensors), 13.4% for element 2 and 5.17% for element 8 (three sensors), respectively.

The results for a three-element damage case are also shown here. The simulated stiffness reductions in the three elements, namely, 2, 5 and 9, are 10.5%, 15%, and 15%, respectively. Using data from five-sensor measurements identifies the stiffness reductions of 10.44%, 14.91%, and 14.90% for elements 2, 5, and 9, respectively, whereas using data from three-sensor measurements identifies the stiffness reductions of 10.46%, 14.97%, and 14.96% for elements 2, 5, and 9, respectively. Some false positive damages are resulted in both single- and multiple-element damage cases. However, the results show that the proposed approach enables good damage identification using a small number of sensors.

Figs. 17–19 show the damage identification results for Scenario 2 with a 10% noise level. The damage prediction results are similar to those of true stiffness reductions. Some false positives with higher values than those in Scenario 1 are observed. The true damage in element 6 is 5%. The prediction results demonstrate using five sensors can provide a stiffness reduction close to the true damage. It is observed that using three sensors can also give quite accurate stiffness reduction, but very few false identification results are also obtained.

Figs. 20–22 show the damage identification results for both single- and multiple-element damage cases in Scenario 3. As in the case of five sensors, the prediction results show a similar pattern, and the results are pretty close to those of true damages with some false positive damage identifications in the undamaged elements. Fig. 20 shows the stiffness reduction in the elements for the single-element damage case. The prediction results in element 4 using three sensors look closer to the true damage than those using five sensors. Still, it is observed that using three sensors gives a higher value of false positives in undamaged elements. The damage identification result for multi-element damage cases shows good results using a few sensors. It can be observed in both Figs. 21 and 22 that the damage prediction results are close to actual damage using both five and three sensors.
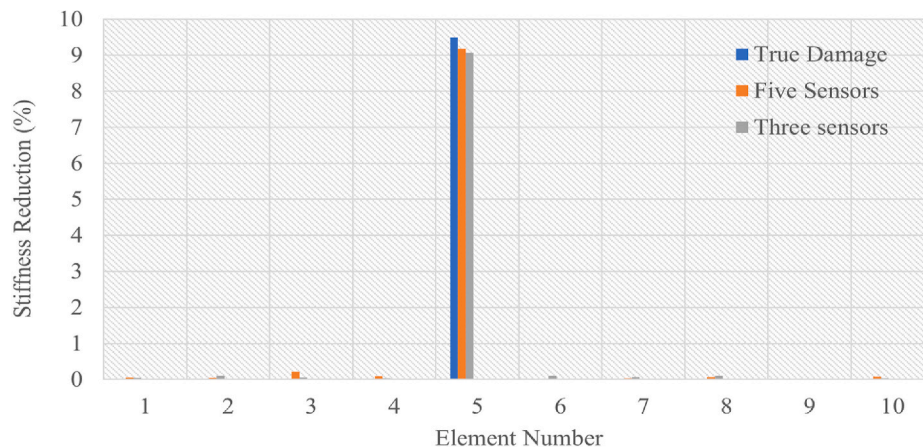
Fig. 14. Damage identification results for a single-element damage case (Scenario 1).
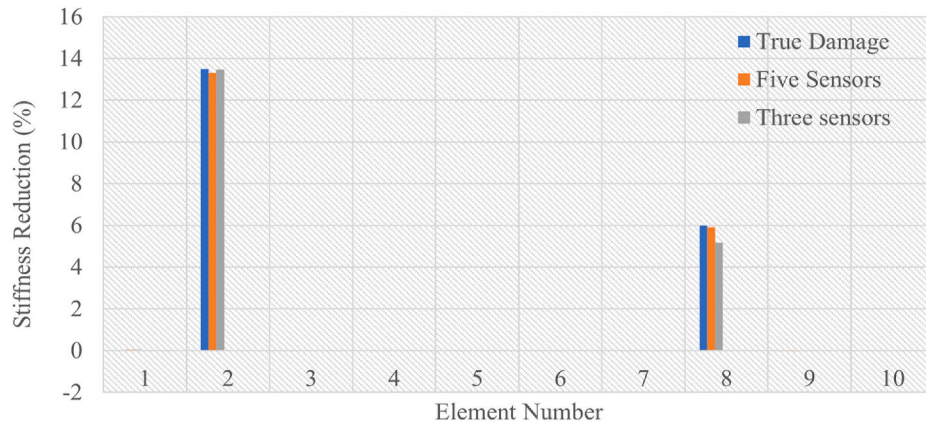
Fig. 15. Damage identification results for a two-element damage case (Scenario 1).

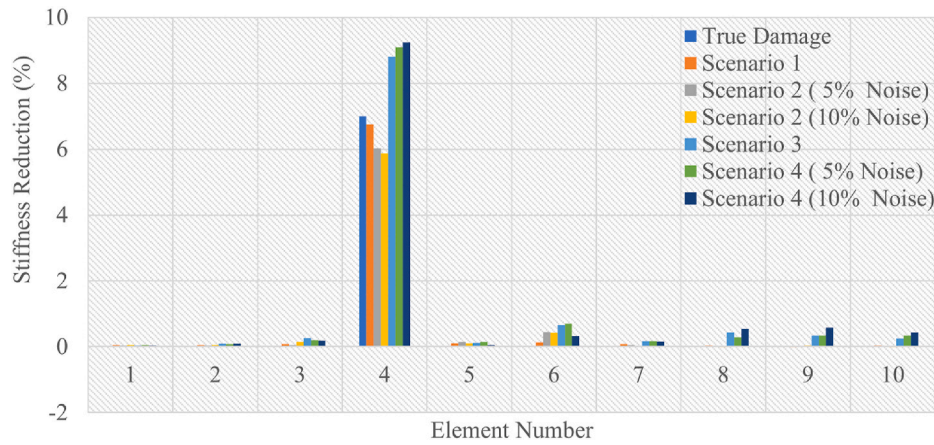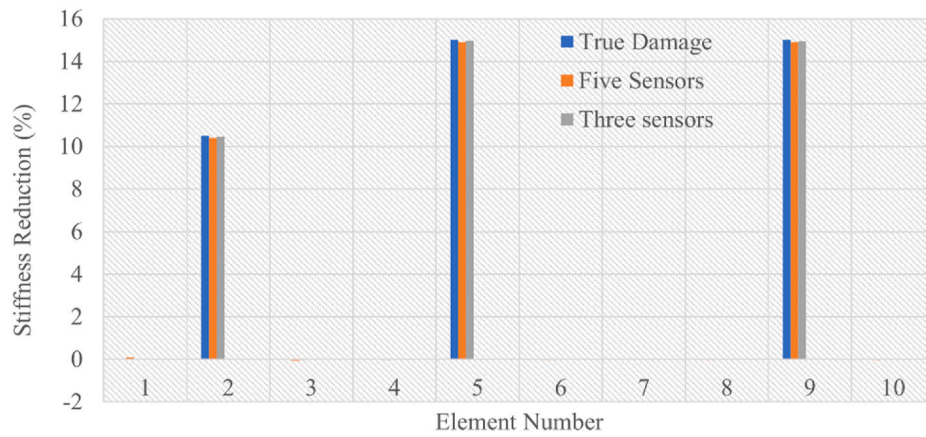**Fig. 16.** Damage identification results for a three-element damage case (Scenario 1).
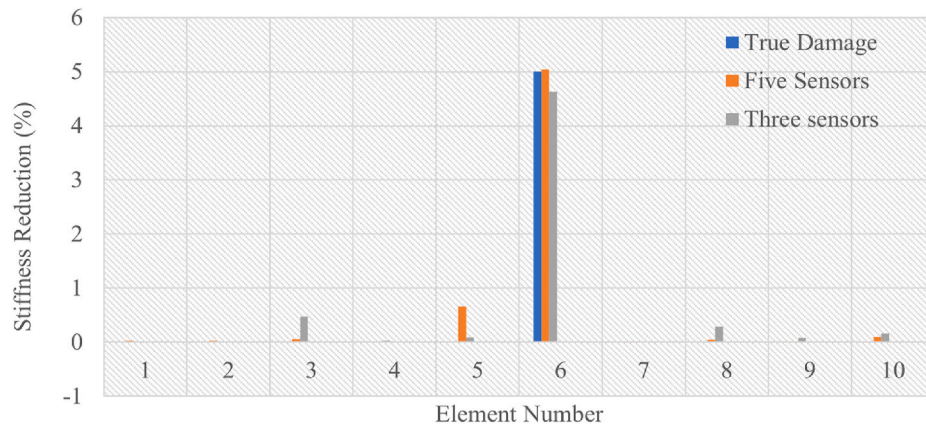
Fig. 17. Damage identification results for a single-element damage case (Scenario 2).
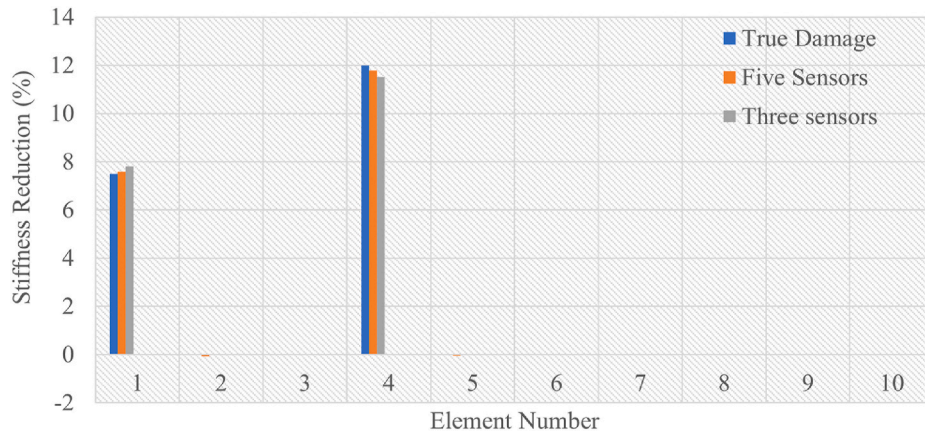
Fig. 18. Damage identification results for a two-element damage case (Scenario 2).
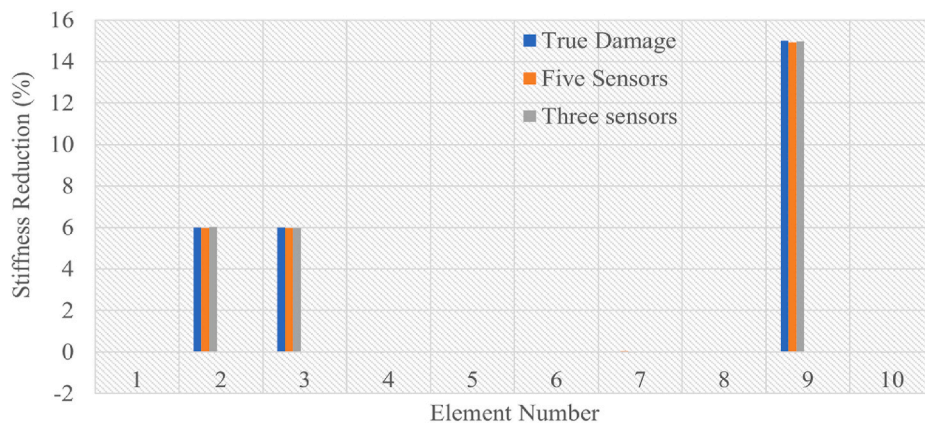
Fig. 19. Damage identification results for a three-element damage case (Scenario 2).
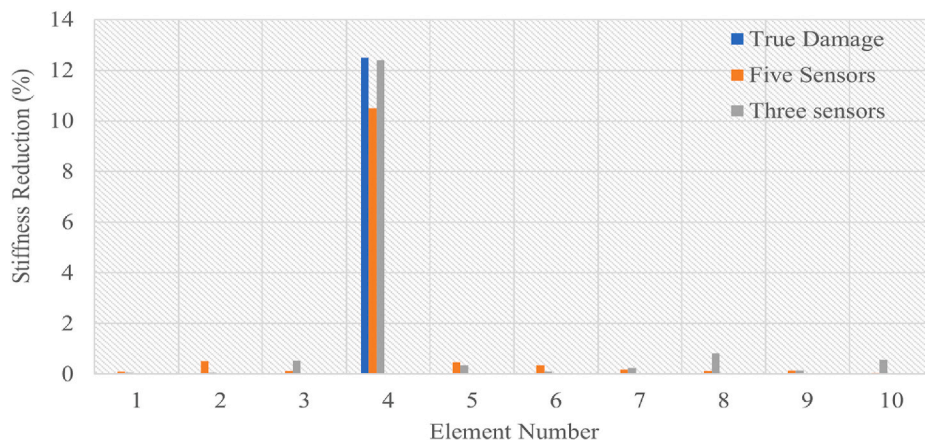
Fig. 20. Damage identification results for a single-element damage case (Scenario 3).
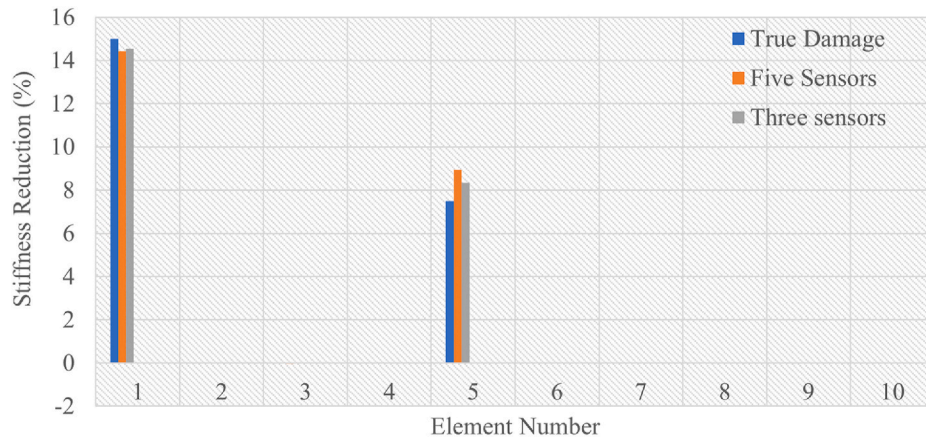
Fig. 21. Damage identification results for a two-element damage case (Scenario 3).
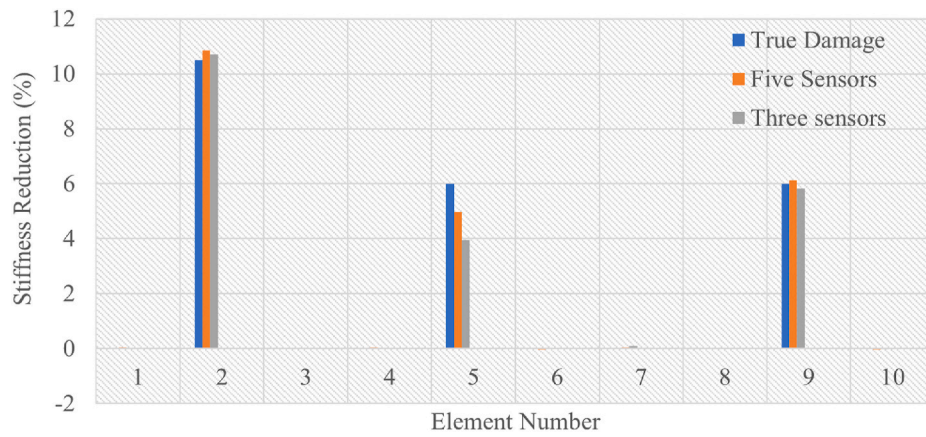
Fig. 22. Damage identification results for a three-element damage case (Scenario 3).
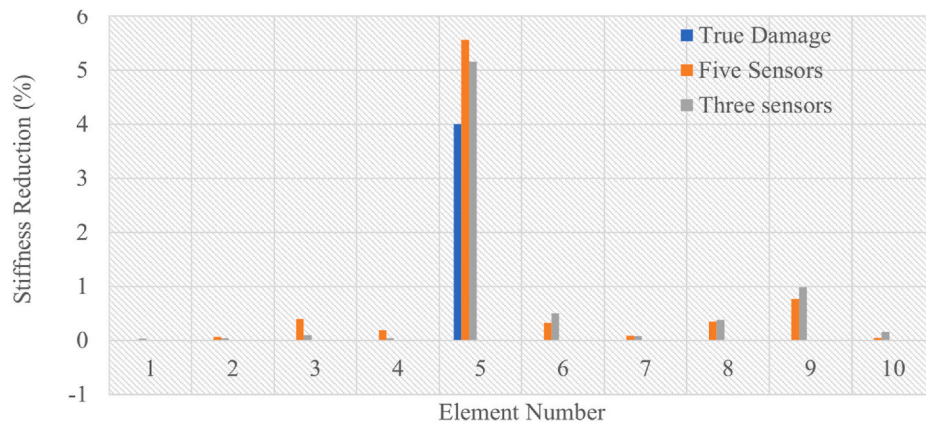
Fig. 23. Damage identification results for a single-element damage case (Scenario 4).
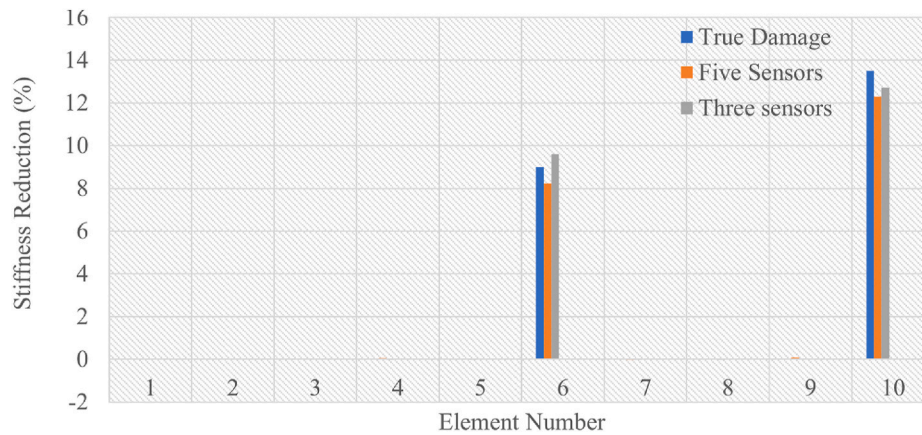
Fig. 24. Damage identification results for a two-element damage case (Scenario 4).
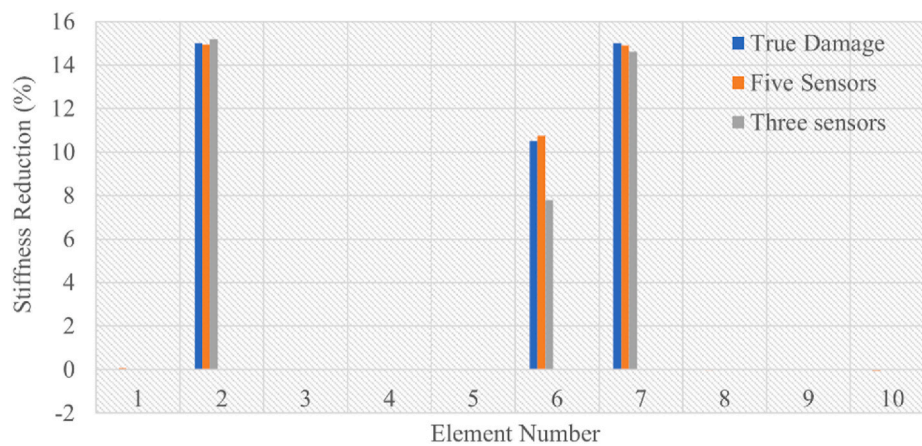
Fig. 25. Damage identification results for a three-element damage case (Scenario 4).

Figs. 23–25 show the damage identification results for Scenario 4 with 10% noise for single-, two-, and three-element damage cases. As observed in previous scenarios, the damage prediction results are close to the true damage results obtained using five sensors. Some false positive damages are observed in the undamaged elements, but the values are less than 1%, which is negligible.

The model implements the same network architecture and pre-processing data methods using five sensors. The damage identification results indicated that the developed model could provide good structural elements identification using a few sensors. The identification results show that even with a reduced number of sensors, the performance of the proposed approach is not significantly affected when the measurement noise and uncertainty in the stiffness parameter are considered. Further, the model is tested with one sensor, but the performance is not good. Therefore, the number of sensors in a practical application can be decided by conducting a numerical study. The measurements from the FEM analysis can be used to train and test the model using a different number of sensors.

6. Conclusions

This paper presents a structural damage identification approach using IRFs and LSTM auto-encoders. The principal components obtained from the concatenated IRFs of the selected sensor locations are used as input sequences. Initially, the LSTM auto-encoder is trained and tuned to reconstruct the input signal. After tuning, the reconstruction network provides a good reconstruction result. The decoder is further tuned for structural damage identification. The proposed approach achieves excellent damage identification performance for all the considered scenarios, and the identification results for both single- and multiple-element damage cases are close to those of the true damage. This study considers noisy measurement and uncertainty in the stiffness parameters. The performance of the proposed approach is further investigated by reducing the number of sensors from five to three. The damage identification results demonstrate that even using three sensors, sufficient information can be obtained using the proposed approach, thereby offering excellent damage identification results. Numerical studies demonstrate good damage identification results. However, experimentation validation will be conducted to validate the results in future.

Declaration of competing interest

The authors declare that they have no known competing financial interests or personal relationships that could have appeared to influence the work reported in this paper.

References

Abdeljaber, O., Avci, O., 2016. Nonparametric structural damage detection algorithm for ambient vibration response: utilizing artificial neural networks and self-organizing maps. J. Archit. Eng. 22 (2), 04016004. https://doi.org/10.1061/(ASCE)AE.1943-5568.0000205.

Abdeljaber, O., Avci, O., Kiranyaz, S., Gabbouj, M., Inman, D.J., 2017. Real-time vibration-based structural damage detection using one-dimensional convolutional neural networks. J. Sound Vib. 388, 154–170. https://doi.org/10.1016/j.jsv.2016.10.043.

Avci, O., Abdeljaber, O., Kiranyaz, S., Hussien, M., Gabbouj, M., Inman, D.J., 2021. A review of vibration-based damage detection in civil structures: from traditional methods to machine learning and deep learning applications. Mech. Syst. Signal Process. 147, 107077. http://doi.org/10.1016/j.ymssp.2020.107077.

Bai, Z., Liu, T., Zou, D., Zhang, M., Zhou, A., Li, Y., 2023. Image-based reinforced concrete component mechnical damage recognition and structural safety rapid assessment using deep learning with frequency information. Autom. Constr. 150, 104839. https://doi.org/10.1016/j.autcon.2023.104839.

Bandara, R.P., Chan, T.H.T., Thambiratnam, D.P., 2013. The three-stage artificial neural network method for damage assessment of building structures. Aust. J. Struct. Eng. 14 (1), 13–25. http://doi.org/10.7158/13287982.2013.11465119.

Betti, M., Facchini, L., Biagini, P., 2015. Damage detection on a three-story steel frame using artificial neural networks and genetic algorithms. Meccanica 50, 875–886. https://doi.org/10.1007/s11012-014-0085-9.

Brownlee, J., 2017. Long short-term memory network with Python: develop sequence prediction models with deep learning (1st ed.). Machine Learning Mastery.

Brownlee, J., 2019. Better deep learning: train faster, reduce overfitting, and make better predictions. Machine Learning Mastery.

Chencho, Li, J., Hao, H., Wang, R., Li, L., 2021. Development and application of random forest technique for element level structural damage quantification. Struct. Control Health Monit. 28 (3), e2678. https://doi.org/10.1002/stc.2678.

Chencho, Li, J., Hao, H., Wang, R., Li, L., 2022. Structural damage quantification using ensemble-based extremely randomised trees and impulse response functions. Struct. Control Health Monit. 29 (10), e3033. https://doi.org/10.1002/stc.3033.

Chollet, F., 2019. The functional API. Retrieved from https://keras.io/guides/functional_api/.

Cury, A., Crémona, C., 2012. Pattern recognition of structural behaviors based on learning algorithms and symbolic data concepts. Struct. Control Health Monit. 19 (2), 161–186. https://doi.org/10.1002/stc.412.

Dackermann, U., Li, J., Samali, B., 2016. Dynamic-based damage identification using neural network ensembles and damage index method. Adv. Struct. Eng. 13 (6), 1001–1016. http://doi.org/10.1260/1369-4332.13.6.1001.

Fallahian, M., Khoshnoudian, F., Meruane, V., 2017. Ensemble classification method for structural damage assessment under varying temperature. Struct. Health Monit. 17 (4), 747–762. https://doi.org/10.1177/1475921717771731.

Fallahian, M., Khoshnoudian, F., Talaei, S., Meruane, V., Shadan, F., 2018. Experimental validation of a deep neural network—sparse representation classification ensemble method. Struct. Des. Tall Special Build. 27 (15), e1504. https://doi.org/10.1002/tal.1504.

Goh, L.D., Bakhary, N., Rahman, A.A., Ahmad, B.H., 2013. Prediction of unmeasured mode shape using neural network for damage detection. Jurnal Teknologi 61 (1), 57–66. https://doi.org/10.11113/jt.v61.1624.

Gui, G., Pan, H., Lin, Z., Li, Y., Yuan, Z., 2017. Data-driven support vector machine with optimization techniques for structural health monitoring and damage detection. KSCE J. Civ. Eng. 21, 523–534. https://doi.org/10.1007/s12205-017-1518-5.

Heng, A., Zhang, S., Tan, A.C.C., Mathew, J., 2009. Rotating machinery prognostics: state of the art, challenges and opportunities. Mech. Syst. Signal Process. 23 (3), 724–739. http://doi.org/10.1016/j.ymssp.2008.06.009.

Hochreiter, S., Schmidhuber, J., 1997. Long short-term memory. Neural Comput. 9 (8), 1735–1780. http://doi.org/10.1162/neco.1997.9.8.1735.

Jardine, A.K.S., Lin, D., Banjevic, D., 2006. A review on machinery diagnostics and prognostics implementation condition-based maintenance. Mech. Syst. Signal Process. 20 (7), 1483–1510. https://doi.org/10.1016/j.ymssp.2005.09.012.

Kan, M.S., Tan, A.C.C., Mathew, J., 2015. A review on prognostic techniques for non-stationary and non-linear rotating systems. Mech. Syst. Signal Process. 62–63, 1–20. https://doi.org/10.1016/j.ymssp.2015.02.016.

Khan, S., Yairi, T., 2018. A review on the application of deep learning in system health management. Mech. Syst. Signal Process. 107, 241–265. https://doi.org/10.1016/j.ymssp.2017.11.024.

Khodabandehlou, H., Pekcan, G., Sami Fadali, M., 2019. Vibration-based structural condition assessment using convolution neural networks. Struct. Control Health Monit. 26 (2), e2308. https://doi.org/10.1002/stc.2308.

Law, S.S., Li, X.Y., 2007. Wavelet-based sensitivity analaysis of the impulse response function for damage detection. J. Appl. Mech. 74 (2), 375–377. https://doi.org/10.1115/1.2189875.

LeCun, Y., Bengio, Y., Hington, G., 2015. Deep learning. Nature 521 (7553), 436–444. https://doi.org/10.1038/nature14539.

Lee, E.W.M., Lam, H.F., 2011. Intelligent-based structural damage detection model. Mech. Adv. Mater. Struct. 18 (8), 590–596. https://doi.org/10.1080/15376494.2011.621838.

Li, J., Hao, H., Fan, X., 2015. Structural damage identification with extracted impulse response functions and optimal sensor locations. Electron. J. Struct. Eng. 14 (1), 123–132. https://doi.org/10.56748/ejse.141961.

Li, P., Zhou, B., Wang, C., Hu, G., Yan, Y., Guo, R., Xia, H., 2024. CNN-based pavement defects detection using grey and depth images. Autom. Constr. 158, 105192. https://doi.org/10.1016/j.autcon.2023.105192.

Li, X.Y., Law, S.S., 2008. Structural damage detection with statistical analysis from support excitation. Mech. Syst. Signal Process. 22 (8), 1793–1808. https://doi.org/10.1016/j.ymssp.2008.03.003.

Lin, J.F., Wang, J., Wang, L.X., Law, S.S., 2019. Structural damage diagnosis-oriented impulse response function estimation under seismic excitations. Sensors 19 (24), 5413. https://doi.org/10.3390/s19245413.

Magalhães, F., Cunha, A., Caetano, E., 2012. Vibration based structural health monitoring of an arch bridge: from automated OMA to damage detection. Mech. Syst. Signal Process. 28, 212–228. https://doi.org/10.1016/j.ymssp.2011.06.011.

Mansouri, M., Avci, O., Nounou, H., Nounou, M., 2015. A Comparative Assessment of Nonlinear State Estimation Methods for Structural Health Monitoring. Conf. Exposition Struct. Dynam. https://doi.org/10.1007/978-3-319-15224-0_5.

Mehrjoo, M., Khaji, N., Moharrami, H., Bahreininejad, A., 2008. Damage detection of truss bridge joints using artificial neural network. Expert Syst. Appl. 35 (3), 1122–1131. https://doi.org/10.1016/j.eswa.2007.08.008.

Ng, C.T., 2014. Application of Bayesian-designed artificial neural networks in Phase II structural health monitoring benchmark studies. Aust. J. Struct. Eng. 15 (1), 27–36. http://doi.org/10.7158/13287982.2014.11465144.

Pathirage, C.S.N., Li, J., Li, L., Hao, H., Liu, W., Ni, P., 2018. Structural damage identification based on autoencoder neural networks and deep learning. Eng. Struct. 172 (1), 13–28. https://doi.org/10.1016/j.engstruct.2018.05.109.

Pathirage, C.S.N., Li, J., Li, L., Hao, H., Liu, W.Q., Wang, R., 2019. Development and application of a deep learning-based sparse autoencoder framework for structural damage identification. Struct. Health Monit. 18 (1), 103–122. https://doi.org/10.1177/1475921718800.

Rafiei, M., Adeli, H., 2018. A novel unsupervised deep learning model for global and local health condition assessment of structures. Eng. Struct. 156 (1), 598–607. https://doi.org/10.1016/j.engstruct.2017.10.070.

Robertson, A., K, P., Alvin, K., 1998. Extraction of impulse response functions data via wavelet transform for structural system identification. J. Vib. Acoust. 120 (1), 252–260. https://doi.org/10.1115/1.2893813.

Sarbu, C., Pop, H., 2005. Principal component analysis versus fuzzy principal component analysis: a case study: the quality of danube water (1985-1996). Talanta 65 (5), 1215–1220. https://doi.org/10.1016/j.talanta.2004.08.047.

Shadan, F., Khoshnoudian, F., Estandiari, A., 2016. A frequency response-based structural damage identification using model updating method. Struct. Control Health Monit. 23 (2), 286–302. https://doi.org/10.1002/stc.1768.

Smarsly, K., Hartmann, D., Law, K.H., 2013. A computational framework for life-cycle management of wind turbines incorporating structural health monitoring. Struct. Health Monit. 12 (4), 359–376. https://doi.org/10.1177/1475921713493344.

Smith, C.B., Hernandez, E.M., 2019. Detection of spatially sparse damage using impulse response sensitivity and LASSO regularization. Inverse Probl. Sci. Eng. 29 (1), 1–16. http://doi.org/10.1080/17415977.2018.1434776.

Vincent, P., Larochelle, H., Lajoie, H., 2010. Stacked denoising autoencoders: learning useful representations in a deep network with a local denoising criterion. J. Mach. Learn. Res. 11 (1), 3371–3408. https://doi.org/10.5555/1756006.1953039.

Wang, R., Chencho, An, S., Li, J., Li, L., Hao, H., Liu, W.Q., 2020. Deep residual network framework for structural health monitoring. Struct. Health Monit. 20 (4), 1443–1461. https://doi.org/10.1177/1475921720918378.

Wang, R., Li, J., Chencho, An, S., Hao, H., Liu, W., Li, L., 2021. Densely connected convolutional networks for vibration based structural damage identification. Eng. Struct. 245, 112871. https://doi.org/10.1016/j.engstruct.2021.112871.

Wang, R., Li, L., Li, J., 2018. A novel parallel auto-encoder framework for multi-scale data in civil structural health monitoring. Algorithms 11 (8), 112. https://doi.org/10.3390/a11080112.

Wang, W., Su, C., 2023. Deep learning-based detection and condition classification of bridge steel bearings. Autom. Constr. 156, 105085. https://doi.org/10.1016/j.autcon.2023.105085.

Wu, R.T., Jahanshahi, M.R., 2018. Data fusion approaches for structural health monitoring and system identification: past, present, and future. Struct. Health Monit. 19 (2), 552–586. https://doi.org/10.1177/1475921718798769.

Xu, X., Yoneda, M., 2021. Multitask air-quality prediction based on LSTM-autoencoder model. IEEE Trans. Cybern. 51 (5), 2577–2586. https://doi.org/10.1109/TCYB.2019.2945999.

Zhang, Y., Qin, C., Srivastava, A.K., Jin, C., Sharma, R.K., 2020. Data-driven day-ahead PV estimation using autoencoder-LSTM and persistence model. IEEE Trans. Ind. Appl. 56 (6), 7185–7192. https://doi.org/10.1109/tia.2020.3025742.

Zhou, X.T., Ni, Y.Q., Zhang, F.L., 2014. Damage localization of cable-supported bridges using modal frequency data and probabilistic neural network. Math. Probl. Eng. 2014, 837963. https://doi.org/10.1155/2014/837963.